Memoirs of the Faculty of Engineering, Okayama University, Vol. 33, No.2, pp. 25-37, March 1999

A Numerical Study on the Performance of an Open-type Flat-plate Solar Collector

Baoyin SONG*, Hideo INABA* and Akihiko HORIBE*

(Received March 1 , 1999)

A set of mathematical models was developed for predicting the performance of an open-type flat-plate solar collector, and solved numerically through an implicit difference method. The effects of various parameters on the absorption of solar energy for the collector were investigated. The results showed that the solar energy absorptance of the open-type flat-plate collector was relatively high especially for the region where the weather was humid and hot, and there were an optimum length and an optimum tilt angle for the absorbing plate on which the collector could obtain the highest solar energy absorptance. It was found that the latent heat flux of water evaporation could be 5 to 15 times larger than the sensible heat flux. The effects of the magnitude of the solar incident flux, the atmospheric humidity, the atmospheric temperature, the absorbing plate tilt angle, and the water film thickness on the temperature rising of the water film were clarified in numerical quantities. The increase of the solar incident flux, the atmospheric humidity or the atmospheric temperature also resulted in a rise in the solar energy absorptance of the collector.

NOMENCLATURE

c mass fraction of water vapor

c_p specific heat [J kg^{-1} K^{-1}]

D mass diffusivity [m^2 s^{-1}]

F local radiation flux [W m^{-2}]

F^o solar radiation flux incident on the gas-water interface [W m^{-2}]

g gravitational acceleration [m s^{-2}]

h_{fg} latent heat of vaporization [J kg^{-1}]

k molecular thermal conductivity [W m^{-1} K^{-1}]

L reference length [m]

$\dot{m}$ interfacial mass flux [kg s^{-1}m^{-2}]

M molar mass [kg kmol^{-1}]

p pressure [Pa]

q_l interfacial latent heat flux in gas side [W m^{-2}]

q_s interfacial sensible heat flux in gas side [W m^{-2}]

q_x total interfacial heat flux [W m^{-2}]

Q_r solar energy incident on the gas-water interface per unit width, F^oL, [W/m]

Q_{wf} net solar energy absorbed by the water film per unit width, $\Gamma c_{pl}\ (T_{out} - T_{in})$, [W/m]

* Department of Mechanical Engineering

R_M universal gas constant [J kmol^{-1} K^{-1}]
T temperature [K]
u, v x-direction and y-direction velocities [m s^{-1}]
x, y coordinates in axial and transverse directions [m]
X dimensionless coordinate in the axial direction, x/L

Greek symbols

α^* absorptivity of surface
β extinction coefficient [cm^{-1}]
γ inter-reflection parameter defined by Eq. (23)
λ wavelength [μm]
λ_c cutoff wavelength beyond which water is opaque to radiation [μm]
ρ density [kg m^{-3}] or reflectivity of surface
δ_l water film thickness [m]
δ_g thickness of velocity boundary layer of gas [m]
μ dynamic viscosity [kg m^{-1} s^{-1}]
ν kinematic viscosity [m^2 s^{-1}]
τ shear stress [Pa] or transmissivity of the gas-water interface
Γ water mass flow rate per unit width [kg m^{-1} s^{-1}]
ψ tilt angle of the absorbing plate [°]

Subscripts

a of dry air
g of gas mixture of dry air and water vapor
i condition at the gas-water interface
in condition at the inlet
l of liquid water
m mean
out condition at the outlet
v of vapor
w condition at the plate surface
λ condition at the wavelength of λ
∞ refers to atmosphere

Superscripts

$+$ refers to the forward direction
$-$ refers to the backward direction
$*$ refers to surface radiation property

1. INTRODUCTION

Solar energy nowadays is widely used to industry, agriculture, science and domestic daily life. Solar collector, solar regenerator, and solar heat pump system are employed in water heating, solution regeneration, space cooling, irrigation and etc[1]. Although thermal collection device has been developed to a rather high level, the open-type flat-plate collector is still used in some fields for its simplest style and low expenses.

The thermal energy transfer in solar collection systems generally includes radiation, convection, conduction and evaporation. In addition to heat transfer, mass transfer occurs simultaneously. An open-type solar collector is a typical gas-liquid system, in which the meteorological quantities, the tilt angle and the absorbing plate length play key roles in heat and mass transfer and the performance of the solar collector. The heat and mass transfer for the gas-liquid system has been studied by many researchers[2–10]. Among them, Yan and Soong[2] investigated the forced convective heat and mass transfer along an inclined heated plate with film evaporation, and Gandhidasan[3] studied the heat and mass transfer in solar regenerators. It is noted that either a forced convective[2,3,5] or a stagnant[4,6,8] gas layer in a gas-liquid flow system is generally focused and a linear distribution of temperature[9] or a negligible temperature gradient[3] across the liquid film has been suggested by some investigators.

The objective of the present work is to investigate the effects of the various parameters, especially meteorolog-

ical quantities such as the magnitude of the solar radiation, the atmospheric temperature and the atmospheric humidity, as well as the geometry conditions including the plate tilt angle and reference length on the solar energy absorption for the collector. A cluster of physical models was developed. The performance of the collector and the characteristics of heat and mass transfer were obtained through solving the equations numerically.

2. ANYLISIS

The physical model concerned in this study is illustrated in Fig. 1. The water falls down a tilted plate as a thin film by the action of gravity. Due to the actions of viscous and inertial forces, the ambient gas will flow along with the water film forming an accompanying boundary layer. The solar radiative flux incident upon the free surface of the water film is partly transmitted across the film and mainly absorbed by the water film and the absorbing plate which has a high solar absorptivity and is perfectly insulated from back. The heat absorbed by the plate then is transferred to the water film and across it to the surrounding gas layer. When evaporation occurs, mass transfer will simultaneously take place between the water film and the gas layer.

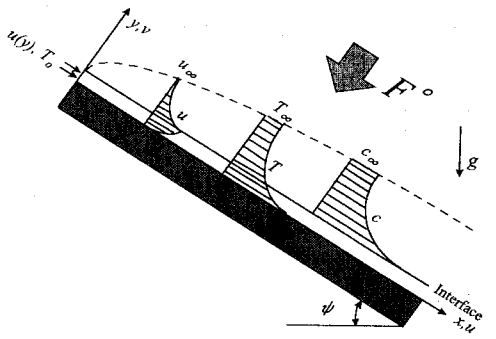

Fig. 1. Schematic diagram of the physical system

2.1 Governing equations

In general liquid film flow is a wavy flow except in the region near the start of flow or at a very small Reynolds number. Besides the statistical approach, nearly all remaining major investigations on the film flow are based on the constant film thickness model for low rate of evaporation[11], which assumes that the film can be treated as smooth so that it can be represented by an average film thickness.

In "the constant film thickness model", assuming the boundary concept to be valid and neglecting the pressure gradient, buoyancy force and dissipated heat, the equations for a steady two-dimensional incompressible laminar flow of the water film are

mass

$$\frac{\partial u_l}{\partial x} + \frac{\partial v_l}{\partial y} = 0 \tag{1}$$

momentum

$$u_l \frac{\partial u_l}{\partial x} + v_l \frac{\partial u_l}{\partial y} = \frac{\partial}{\partial y}\left(\nu_l \frac{\partial u_l}{\partial y}\right) + g \sin\psi \tag{2}$$

and energy

$$\rho_l c_{pl} u_l \frac{\partial T_l}{\partial x} + \rho_l c_{pl} v_l \frac{\partial T_l}{\partial y} = \frac{\partial}{\partial y}\left(k_l \frac{\partial T_l}{\partial y}\right) + \frac{\partial}{\partial y}\left(F^+ - F^-\right) \tag{3}$$

where F^+ and F^- are the radiative fluxes in the forward (+) and backward (−) directions in the water film, respectively, and will be modeled later. The second term on the right side of Equation (3) represents the energy transfer due to the film absorption of the solar radiation. The radiative flux gradient acts like a source which has been neglected in the analysis of Gandhidasan[3].

Neglecting the gas absorption of the solar radiation, then the equations of mass, momentum, energy and

concentration in the accompanying gas boundary layer can be induced as

$$\frac{\partial(\rho_g u_g)}{\partial x} + \frac{\partial(\rho_g v_l)}{\partial y} = 0 \tag{4}$$

$$\rho_g u_g \frac{\partial u_g}{\partial x} + \rho_g v_g \frac{\partial u_g}{\partial y} = \frac{\partial}{\partial y}\left(\mu_g \frac{\partial u_g}{\partial y}\right) + g\,(\rho_g - \rho_\infty)\sin\psi \tag{5}$$

$$\rho_g c_{pg} u_g \frac{\partial T_g}{\partial x} + \rho_g c_{pg} v_g \frac{\partial T_g}{\partial y} = \frac{\partial}{\partial y}\left(k_g \frac{\partial T_g}{\partial y}\right) + \rho_g D(c_{pv} - c_{pa}) \frac{\partial c}{\partial y}\frac{\partial T_g}{\partial y} \tag{6}$$

and

$$\rho_g u_g \frac{\partial c}{\partial x} + \rho_g v_g \frac{\partial c}{\partial y} = \frac{\partial}{\partial y}\left(\rho_g D \frac{\partial c}{\partial y}\right) \tag{7}$$

The second term on the right side of Equation (6) represents the transport of energy due to the concentration gradient which has not been considered in the analysis of Yan and Soong[2]. Furthermore, it is assumed that the gas mixture exhibits ideal gas law behavior. Neglecting the instantaneous values, the thermal equation of state is written as

$$p_g = \rho_g T_g R_M \left(\frac{1-c}{M_a} + \frac{c}{M_v}\right) \tag{8}$$

and the specific heat for the binary gas mixture becomes

$$c_{pg} = c_{pa} + c(c_{pv} - c_{pa}) \tag{9}$$

where c_{pa} and c_{pv} denote the specific heats for dry air and water vapor, respectively.

2.2 Boundary and interfacial conditions

The boundary conditions for the problem are

$$x = 0 \;:\quad u_l = u(y),\;\; T_l = T_{in},\;\; u_g = 0,\;\; T_g = T_\infty,\;\; c = c_\infty \tag{10}$$

$$y = 0 \;:\quad u_l = 0,\;\; -k_l \frac{\partial T_l}{\partial y} = \int_0^{\lambda_c} \alpha^*_{w\lambda} F^+_\lambda(0)\mathrm{d}\lambda \tag{11}$$

and

$$y \to \infty \;:\quad u_g = 0,\;\; T_g = T_\infty,\;\; c = c_\infty \tag{12}$$

The term on the right side of Equation (11) accounts for the absorption of the solar radiation by the opaque plate.

At the gas-water interface (y=δ_l), the continuities of velocity, temperature, and shear stress, and the energy balance must be met as follows:

$$u_i = u_l = u_g \tag{13}$$

$$T_i = T_l = T_g \tag{14}$$

$$\tau_i = \left[\mu_l \frac{\partial u_l}{\partial y}\right]_{i,l} = \left[\mu_g \frac{\partial u_g}{\partial y}\right]_{i,g} \tag{15}$$

$$\int_{\lambda_c}^{\infty} \alpha^*_{i\lambda} F^o_\lambda \mathrm{d}\lambda - \left[k_l \frac{\partial T_l}{\partial y}\right]_{i,l} = h_{fg}\dot{m} - \left[k_g \frac{\partial T_g}{\partial y}\right]_{i,g} \tag{16}$$

By considering the solubility of air in the water film negligibly small, the transverse velocity of the air-vapor mixture at the gas-water interface can be

$$v_i = -\left[\frac{D}{1-c}\frac{\partial c}{\partial y}\right]_{i,g} \tag{17}$$

and the mass flux from the water film to the gas layer leads to

$$\dot{m} = \rho_{gi} v_i \tag{18}$$

Assuming the gas-water interface at the saturation pressure of water vapor, p_{vi}, the interfacial mass fraction of water vapor can be evaluated by[12]

$$c_i = \frac{p_{vi}}{(p_\infty - p_{vi})\frac{M_a}{M_v} + p_{vi}} \tag{19}$$

where M_a and M_v denote the molar mass of air and vapor, respectively. The partial pressure of the saturation water vapor at the gas-water interface is estimated from Antoine's correlation[13]

$$p_{vi} = 133.32 \exp\left(18.304 - \frac{3816.4}{T_i - 46.130}\right) \tag{20}$$

2.3 Radiative transfer model

Both gas and water are semitransparent to radiation. They are transparent in the visible and infrared part of the spectrum, and scattering is negligible in comparison to absorption. It is assumed in analysis that the absorption of the solar radiation in the gas layer is negligibly small, and the interfaces are smooth. Then the radiative heat fluxes in the forward (+) and backward (−) directions in the water film (Fig.2) can be expressed as[14]

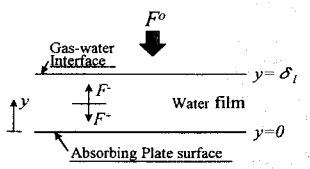

Fig. 2. Schematic of the radiation model

$$F^+ = \int_0^{\lambda_c} F_\lambda^+(y)\mathrm{d}\lambda = \int_0^{\lambda_c} \tau_\lambda^* F_\lambda^o \mathrm{e}^{-\beta_\lambda(\delta_l - y)}\gamma_\lambda \mathrm{d}\lambda \tag{21}$$

and

$$F^- = \int_0^{\lambda_c} F_\lambda^-(y)\mathrm{d}\lambda = \int_0^{\lambda_c} \rho_{w\lambda}^* \tau_\lambda^* F_\lambda^o \mathrm{e}^{-\beta_\lambda(\delta_l + y)}\gamma_\lambda \mathrm{d}\lambda \tag{22}$$

respectively. In these equations

$$\gamma_\lambda = [1 - \rho_{w\lambda}^* \rho_{i\lambda}^* \exp(-2\beta_\lambda \delta_l)]^{-1} \tag{23}$$

is a parameter which accounts for inter-reflection of radiation between the gas-water interface and the absorbing surface.

2.4 Thermodynamic, transport and radiation properties

The variations of thermodynamic and transport properties with temperature and mixture composition in our study are considered. The transport properties for air[15] are used as follows:

$$\mu_a = \frac{14.58 \times 10^{-7} T^{\frac{3}{2}}}{110.4 + T} \tag{24}$$

$$k_a = \frac{2.648 \times 10^{-3} T^{\frac{3}{2}}}{T + 245.4 \times 10^{-\frac{12}{T}}} \tag{25}$$

$$c_{pa} = 917 + 0.258T - 3.98 \times 10^{-5}T^2 \quad (26)$$

Other pure property data and the mixture properties are estimated from Reid et al[13].

Water is selective absorber of radiation and its volumetric radiation property was taken from Brewster[16]. The cutoff wavelength for water, λ_c, is assumed to be 2.5 μm. The radiation surface properties of water and the plate were taken from available literature sources[12,16,17].

3. SOLUTION METHOD

A control-volume finite-difference procedure[18] was used to solve the coupling equations. A fully implicit numerical scheme was employed. The convective term was approximated by power-law form, and a total of 151 $\times$1202 grids was used across the water film and gas layer thickness in view of the study performed by Yan and Soong[2].

The system of algebraic discretization equations obtained for the water and gas regions was solved through the line-by-line application of the tri-diagonal matrix algorithm. It is noted that at the gas-water interface the matching discretization equations were set up by making momentum and energy balances. To avoid divergence of iterations, the time interval in the discretization equations for unsteady problems was chosen as a specific under-relaxation factor to solve our steady problem.

The total radiation fluxes were evaluated numerically using a spectral-band model. A total of only 21 spectral bands was used because a more detailed spectral distribution of incident radiation flux was not available[19].

4. RESULTS AND DISCUSSION

The solar incident flux, the atmospheric humidity and temperature, the absorbing plate tilt angle and its length, and the water film thickness are important parameters concerned in this study. Solar flux incident on the earth outside the atmosphere is 1390 W/m^2. At the surface of the earth the flux is somewhat less due to atmospheric absorption and scattering. On a clear day and for moderate (near normal) slant paths through the atmosphere, the actual incident flux at the ground is closer to 1190 W/m^2 [16]. However for different geographic region, in different season, at different solar time and on specific weather condition, the value of the solar flux incident on the terrestrial surface certainly varies a lot[1,20]. The atmospheric humidity and temperature are mainly influenced by the local water surface area and climate condition[20]. The orientation of the solar energy collecting surface with respect to the direction of incidence is extremely important to the performance of any solar energy system. The absorbing plate tilt angle generally depends on the local latitude and solar time. Some useful rules of thumb indicate that the optimum tilt for flat-plate collectors which are mounted in stationary position and used in a year-round mode is an angle equal to that of the local latitude. For only winter using, the tilt angle should be steeper to catch the lower winter sun, and equal to the local latitude plus 15° [1]. The absorbing plate length for the solar collector can be chosen and however it is limited by the space and its base. Based on above consideration, we chose the ranges of the parameters in this study as: $15° \leq \psi \leq 60°$, 0 W/m^2 $\leq F^o \leq$ 1190 W/m^2, 5×10^{-4} m$\leq \delta_l \leq 7.5 \times 10^{-4}$ m, 288 K$\leq T_\infty \leq$ 298 K, $0.003 \leq c_\infty \leq 0.014$, $T_{in} = 293.15$ K and 1 m $\leq L \leq$ 3 m.

Figure 3 shows the typical transverse (y-direction) distributions of the water flow velocity and temperature at

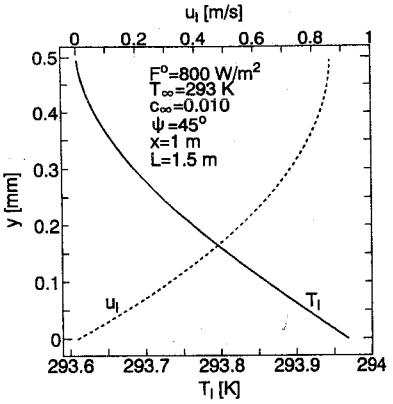

Fig. 3. Typical transverse distributions of water flow velocity and temperature

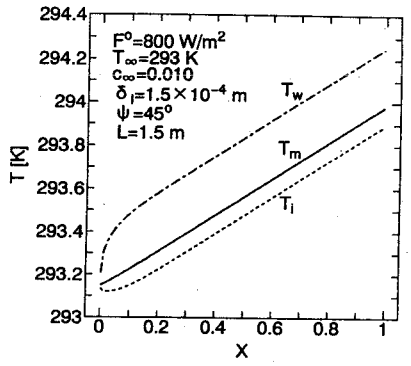

Fig. 4. Axial distributions of T_m, T_w and T_i on specific conditions

$x = 1$ m. The data show that the profile of water flow velocity, u_l, is somewhat parabolic but the distribution of temperature, T_l, is non-linear.

Typical axial distributions of the mean water film temperature, T_m, the absorbing plate surface temperature, T_w, and the gas-water interfacial temperature, T_i, are plotted in Fig. 4. The mean water film temperature is calculated by

$$T_m = \frac{1}{\delta_l u_m} \int_0^{\delta_l} u_l T_l \mathrm{d}y \tag{27}$$

where

$$u_m = \frac{1}{\delta_l} \int_0^{\delta_l} u_l \mathrm{d}y \tag{28}$$

is the mean x-direction water velocity. As expected, continuous radiant heating under the solar incident flux of F^o=800 W/m^2 raises all T_m, T_i and T_w along the flow direction except the very short region near the inlet in which the high evaporation rate makes the interface temperature drop somewhat to keep energy balance.

Figure 5 presents the transverse distributions of temperature and the mass fraction of water vapor at two different x positions, respectively. At x=1 m (boundary layer developed region), both the temperature and the mass fraction of water vapor in gas boundary layer decrease with an increase in y. At $x = 0.065$ m (entrance region), the mass fraction of water vapor drops suddenly near the interface but the temperature of air-vapor mixture first rises to its maximum at around y=3 mm and latter gradually reduces to the value of atmosphere (T_∞=293 K). This can be explained by the fact that the water vapor carrying a lot of heat from the gas-water interface releases heat with its mass fraction sharply decreasing on the way outside, which causes the gas temperature to rise to the maximum at some position in earlier developing region. The energy transport due to the concentration gradient has been revealed in the second term on the right side of Eq. (6).

The interfacial mass fraction of water vapor, c_i, is a function of the interfacial temperature, T_i, *i.e.* $c_i = f(T_i)$. Therefore, the developing tendency of the interfacial mass fraction of water vapor is similar to that of the interfacial temperature, which can be understood by contrasting Fig. 6 with Fig. 4. For F^o=0 W/m^2, since the evaporation and sensible heat transfer take heat from the water film, the interfacial temperature has no way of rising but dropping, and the interfacial mass fraction of water vapor therefore decreases with an increase in X. The increase of the magnitude of the solar incident flux helps the temperature of the water film rise more

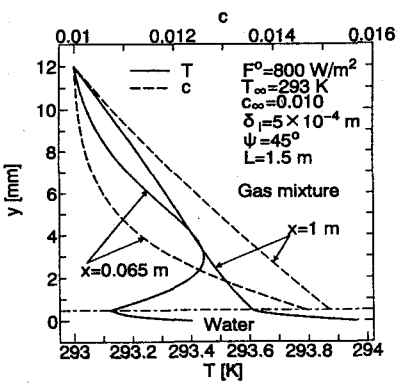

Fig. 5. Transverse distributions of temperature and the mass fraction of water vapor at two x positions

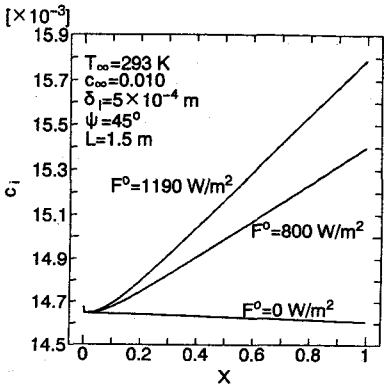

Fig. 6. Effect of radiative flux on the interfacial mass fraction of water vapor

quickly along the flow direction. The interfacial mass fraction of water vapor therefore reaches a higher value at the outlet of X=1.

The mass and heat fluxes at the gas-water interface are the most dominant parameters for heat and mass transfer from the water film to the gas layer. The total interfacial heat flux, q_x, consists of two parts that one is sensible heat flux, q_s, and the other is latent heat flux, q_l. It can be expressed as

$$q_x = q_l + q_s = h_{fg}\dot{m} - \left[k_g \frac{\partial T_g}{\partial y}\right]_{i,g} \tag{29}$$

The variation of interfacial mass flux, $\dot{m}$, with dimensionless coordinate X, and the effect of the mass fraction of water vapor in ambient atmosphere, c_∞, on it are shown in Fig. 7. The interfacial mass flux first drops suddenly from a very high value at the inlet of X=0 to a certain value of around constant for later development at some specific position for different atmospheric mass fraction of water vapor, which should be attributed to the development of the concentration boundary layer. For c_∞=0.014 (the relative humidity, RH, is about 96%), the drop of the interfacial mass flux in the entrance region near the inlet of water film flow is rather steep and the value of the interfacial mass fraction in the developed region is quite small. But for a smaller c_∞, the drop of the interfacial mass flux of water vapor will slow down and its value will be higher. This phenomenon is easy to understand by the fact that the high humid weather condition makes the concentration boundary layer difficult to develop and the water film hard to evaporate. Adversely the low atmospheric humidity would help the concentration boundary layer to develop and the water film to evaporate.

Figure 8 shows the variations of dimensionless heat flux q_l/F^o and q_s/F^o with demensionless coordinate X for different c_∞. The variation of q_l/F^o with X is quite similar to that of $\dot{m}$, which could be attributed to that q_l is the function of $\dot{m}$. The maximum gas temperature resulted in by lower atmospheric humidity (see Fig. 5) causes negative sensible heat flux in the entrance region. The sensible heat flux under the lower atmospheric humidity grows so quickly that it will exceed the value on the condition of a higher atmospheric humidity at a certain position. When the mass fraction of water vapor in ambient atmosphere, c_∞, is 0.014 (RH = 96%), the heat loss rate from the water film is only about 2.4% of the incident radative flux in the developed region. However as c_∞ reduces to 0.003 (RH = 21%), q_x/F^o reaches a value around 13%. The interfacial latent heat

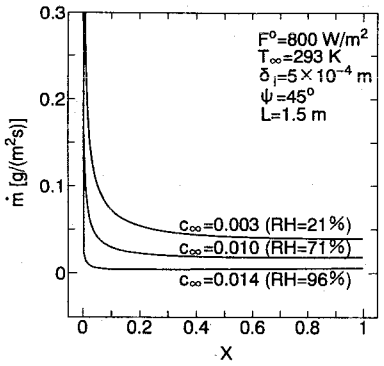

Fig. 7. Effect of atmospheric humidity on the water film evaporation

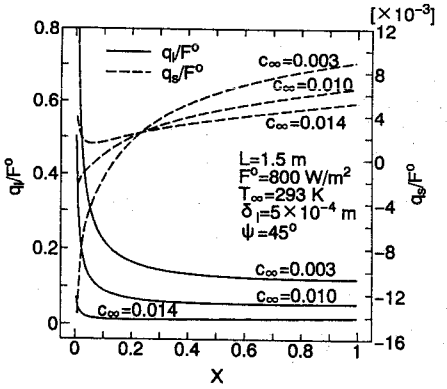

Fig. 8. Effects of atmospheric humidity on sensible and latent heat transfers

flux, q_l, is a dominant fraction of the total interfacial heat flux, q_x. Its value can be 5 to 15 times larger than that of the interfacial sensible heat flux, q_s.

The axial distribution of the mean water film temperature reflects the performance of the solar energy collecting system. The data in Figs. 9–12 show that the mean water film temperature, T_m, rises or drops (for F^o =0 W/m ^{2}) almost linearly along the axial direction except in the entrance region of water flow in which the high evaporation rate slows down its rising. Any increase of the atmospheric humidity, the magnitude of the solar incident flux or the atmospheric temperature will certainly enhance the film temperature rising. This is explained by the fact that the energy of water heating is mainly from the solar incident flux, and the energy loss of the water film is by means of latent and sensible heat transfer. The amount of latent heat transfer is generally much higher than that of sensible heat transfer. Therefore the effect of the atmospheric humidity on the mean water film temperature is more marked than that of the atmospheric temperature. The effect of the absorbing plate tilt angle on the mean water film temperature shown in Fig. 12 could reveal that the decrease of the tilt angle reduces the water flow velocity, which allows the water to be heated for a longer period.

The film temperature difference between the outlet and inlet of the solar energy collecting plate is another important parameter for the performance of the collector. Figures 13–14 provide the effects of the solar incident

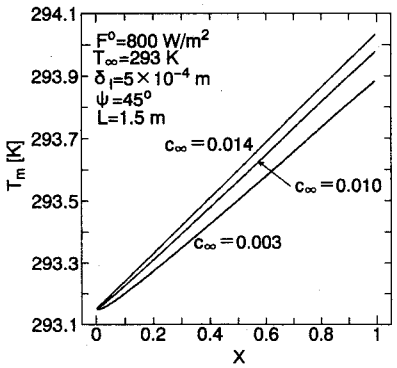

Fig. 9. Effect of atmospheric humidity on mean water film temperature

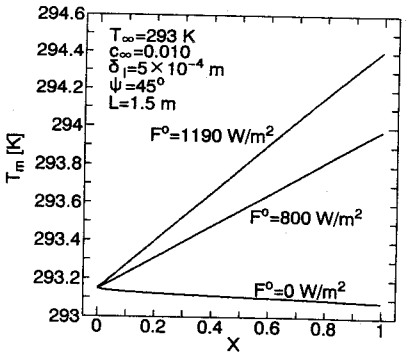

Fig. 10. Effect of radative flux on mean water film temperature

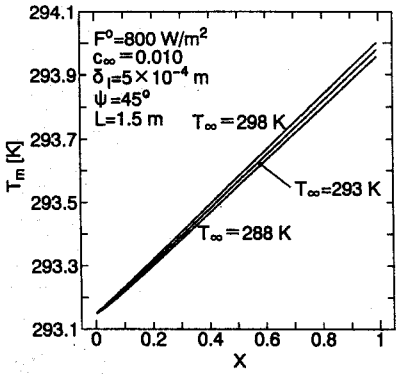

Fig. 11. Effect of atmospheric temperature on mean water film temperature

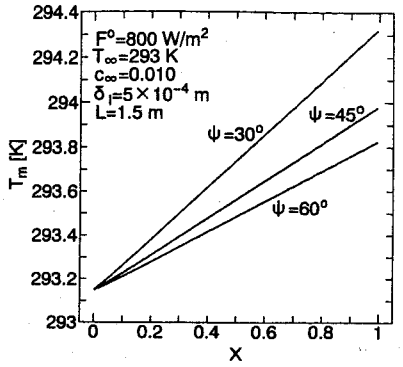

Fig. 12. Effect of plate tilt angle on mean water film temperature

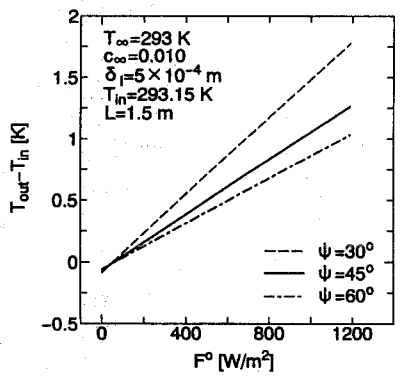

Fig. 13. Effects of radiative flux and the plate tilt angle on the water film temperature rise

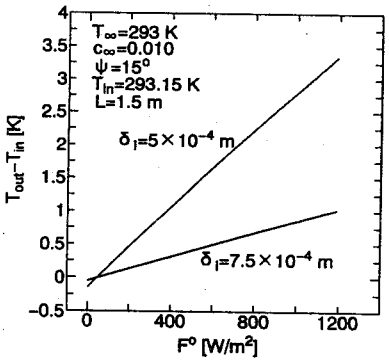

Fig. 14. Effects of radiative flux and the film thickness on the water film temperature rise

flux, F^o, the plate tilt angle, ψ, and the water film thickness, δ_l, on the water film temperature rise, $T_{out} - T_{in}$, respectively. The obtained results reveal that the outlet water film temperature will linearly increase with increasing the solar incident flux. Any decrease of the tilt angle or the water film thickness will further raise the outlet water film temperature except for F^o=0 W/m^2. The decrease of the tilt angle reduces the water flow velocity, which allows the water to be heated for a longer period as it flows from the inlet to the outlet. The decrease of the film thickness markedly decreases the heat capacity of the water film so that the mean outlet water temperature rises to a higher value. However on the condition of no solar radiation available such as during the night, the decrease of mean water flow velocity which is caused by means of decreasing the tilt angle or the film thickness will make the water take a longer time to flow across the plate and loss more heat so that the mean outlet water temperature drops to a lower value.

What we are most interested in is how much the solar energy incident on the free surface of the water film was absorbed by the water film. Therefore the ratio of the net energy absorbed by the water film to the solar energy incident on the free surface of the water film, Q_{wf}/Q_r, is the most important parameter in this study. The increase of the atmospheric humidity or the atmospheric temperature causes Q_{wf}/Q_r to rise linearly, as shown in Fig. 15. This can be explained by the fact that the increases of the atmospheric humidity and temperature

reduce the concentration and temperature gradients in the gas boundary layer, which limits the latent and sensible heat transfer from the water film to the gas boundary layer and even allows the sensible heat to be transferred from the gas boundary layer to the water film as the temperature gradient becomes negative. Figure 16 presents the effects of the solar incident flux on the net solar energy absorbed by the water film, and the ratio of the net absorbed energy to the solar energy incident on the gas-water interface. The data reveal that the net energy absorbed by the water film increases almost linearly with an increase in solar incident flux, but not the ratio. As mentioned above, the heat loss of the water film mainly depends on the atmospheric humidity and temperature. Therefore Q_{wf}/Q_r keeps a lower value for a lower solar incident flux and raises its value at variable rates as the solar incident flux increases. Unlike the variation of Q_{wf}/Q_r with c_∞, T_∞, or F^o, which is linear or monotonic, the variation of Q_{wf}/Q_r with the plate tilt angle, ψ, or the plate length, L, has a maximum at about $\psi = 26°$, and $L = 2.2$ m, respectively, which is shown in Fig 17. For a larger tilt angle the water flow velocity reaches a higher value, which enhances the heat transfer between the water film and the gas boundary layer. When the tilt angle is chosen as a smaller value the gas-water interfacial temperature along the flow direction rises so quickly that the higher temperature gradient in the gas boundary layer will enhance the energy loss of the water film. For the shorter absorbing plate length, the high heat transfer between the water film and the gas boundary layer in the earlier boundary layer developing region plays an important role. The influence of the boundary layer thickness on the heat loss of the water film reduces and the water film temperature rising along the axial direction plays more roles on the heat loss with an increase in the plate length. It is noted that among the loss of the solar incident energy which varies from 13% to 28%, about one third to a half is the reflected energy which depends on the radiation surface properties of the water and the plate.

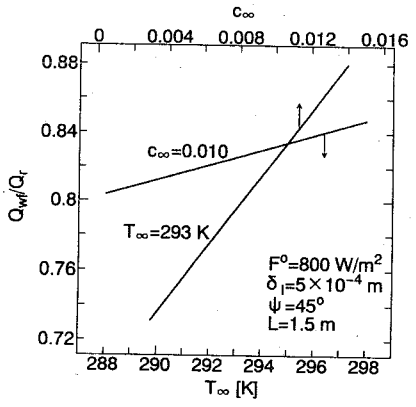

Fig. 15. Effect of atmospheric temperature or humidity on solar energy absorption

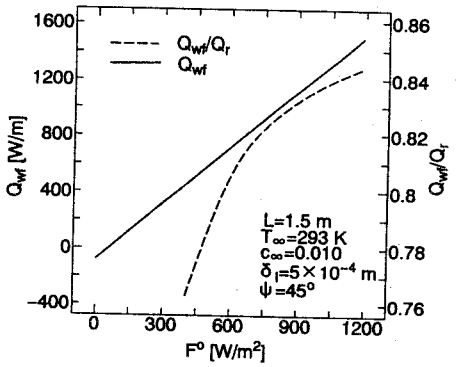

Fig. 16. Effect of radiative flux on solar energy absorption

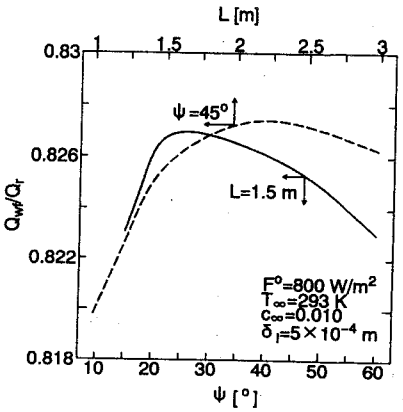

Fig. 17. Effect of the plate tilt angle and length on solar energy absorption

5. CONCLUSIONS

The solar energy absorption performance and the heat and mass transfer characteristics of an open-type flat-plate collector have been studied numerically in this paper. The effects of weather and geometry conditions on them were investigated. From the results and discussion, the following conclusions could be drawn

(1) an optimum length and an optimum tilt angle for the absorbing plate on which the collector could obtain the highest solar energy absorptance were determined in present study.

(2) The latent heat flux was 5 to 15 times larger than sensible heat flux. Therefore the mass transfer among the heat and mass transfers were dominant factor. It mainly controlled the amounts of water evaporation and heat loss of the heated water film.

(3) The effects of the magnitude of the solar incident flux, the atmospheric humidity and temperature, the plate tilt angle, and the water film thickness on the temperature rising of the water film were clarified in numerical quantities.

(4) The lower atmospheric humidity resulted in a maximum temperature value at a certain position of the gas boundary layer in the entrance region.

ACKNOWLEDGEMENTS

The financial support of this work by the Patedison Co. Ltd with Mr. Takashi Takahashi serving as the president is greatly acknowledged. The first author is a visiting scholar from the People's Republic of China. He is grateful to the China Flight Test Establishment (Xi'an, China) for supporting him during the course of this study.

REFERENCES

(1) P. N. Cheremisinoff, P.E. and T. C. Regino: Principles & Applications of Solar Energy, Ann Arbor Science, (1978).

(2) W. M. Yan and C. Y. Soong: Int. J. Heat Mass Transfer, 38, (1995),1261.

(3) P. Gandhidasan: Handbook of Heat and Mass Transfer, Vol. 2, ed. N. P. Cheremisinoff, Gulf Publishing Company, (1986), 1475.

(4) T. D. Karapantios, M. Kostoglou and A. J. Karabelas: Int. J. Heat Mass Transfer, 38, (1995), 779.

(5) J. Schröppel, F. Thiele and O. Unterlöhner: Numerical Methods in Thermal Problems, Vol. II, eds. R. W. Lewis, K. Morgan and B. A. Schrefler, Pineridge press, (1981), 1215.

(6) A. Faghri: Numerical Methods in Thermal Problems, Vol. III, eds. R. W. Lewis, J. A. Johnson and W. R. Smith, Pineridge press, (1983), 980.

(7) R. Yang and D. Jou: Int. J. Heat Mass Transfer, 38, (1995), 1121.

(8) G. Grossman: Handbook of Heat and Mass Transfer, Vol. 2, ed. N. P. Cheremisinoff, Gulf Publishing Company, (1986), 211.

(9) Y. Fujita and M. Tsutui: Trans. JSME, (**B**), 60, (1994), 3469 (in Japanese).

(10) T. Kumada: Handbook of Heat and Mass Transfer, Vol. 1, ed. N. P. Cheremisinoff, Gulf Publishing Company, (1986), 231.

(11) S. M. Yih: Handbook of Heat and Mass Transfer, Vol. 2, ed. N. P. Cheremisinoff, Gulf Publishing Company, (1986), 111.

(12) E. R. G. Eckert and R. M. Drake, Jr.: Analysis of Heat and Mass Transfer, McGraw-Hill Kogakusha, (1972).

(13) R. C. Reid, J. M. Prausnitz and T. K. Sherwood: The Properties of Gases and Liquids, 3rd edition, McGraw-Hill, (1977).

(14) B. Song and R. Viskanta: AIAA J. Thermophysics, 4, (1990), 311.

(15) Z. Y. Zhong, K. T. Yang and J. R. Lloyd: Numerical Methods in Heat Transfer, Vol.III, ed. R. W. Lewis and K. Morgan, John Wiley & Sons, (1985), 195.

(16) M. Q. Brewster: Thermal Radiative Transfer and Properties, John Wiley & Sons, (1992).

(17) V. J. Lunardini: Heat Transfer in Cold Climates, Van Nostrand Reinhold, (1981), 228.

(18) S. V. Patankar: Numerical Heat Transfer and Fluid Flow, Hemisphere/McGraw-Hill, (1980).

(19) B. W. Webb: Radiation induced Melting of Semitransparent materials, Ph.D. Thesis, Purdue University, (1986).

(20) Japanese National Astronomical Observatory (ed.): Chronological Scientific Tables, Maruzen Co., Ltd., (1994), (in Japanese).